3D reconstruction of erupting filaments with STEREO data

Ting Li[1] and Jun Zhang[1]

[1]Key Laboratory of Solar Activity, National Astronomical Observatories, Chinese Academy of Sciences, Beijing 100012, China; [liting;zjun]@nao.cas.cn

Abstract. The launch of *STEREO* spacecraft in October 2006 provided an opportunity to view filament eruptions from two viewpoints giving new insights into their three-dimensional (3D) geometry and true trajectory. The kinematical parameters (velocity and acceleration vectors), the rotation motion, non-radial motion and the helical twist around the filament axis in 3D space have been obtained for the first time. All these properties of erupting filaments are very important to our understanding of the physical phenomena triggering the eruption and their early evolution. In the present paper we review different reconstruction techniques of erupting filaments and the main results obtained using the *STEREO* observations.

Keywords. filaments, coronal mass ejections (CMEs), flares, etc.

1. Introduction

The study of filament eruptions is of great significance because of their close association with coronal mass ejections (CMEs). In the outer corona, CMEs are generally observed to have a three-part structure: the bright core, the dark cavity, and the leading edge (see, e.g., Illing & Hundhausen 1986). The bright core is thought to be composed of filament material. In the inner corona, the filament is located within a flux rope which is the pre-eruption structure of a CME (Li & Zhang 2013).

The eruption mechanism is still unclear although a large number of studies about the nature of filament eruptions and CMEs have been carried out (Filippov 2013; Jiang *et al.* 2011; Liu *et al.* 2012; Shen *et al.* 2012). According to these studies, ideal MHD instabilities such as the kink instability (Fan 2005; Török & Kliem 2005) and the torus instability (Kliem & Török 2006) are thought as one type of eruption mechanism. Other eruption mechanisms include "tether cutting" model (Sturrock 1989; Moore *et al.* 2001) and "break out" model (Antiochos *et al.* 1999; Gilbert *et al.* 2007), both of which focus on magnetic reconnection as the driver of eruption. The kinematic properties of erupting filaments are very important to our understanding of the associated physical mechanisms.

According to previous studies, filaments often exhibit a relatively slow rise ("slow-rise phase") prior to eruption (e.g., Tandberg-Hanssen *et al.* 1980; Kahler *et al.* 1988). For quiet-region events, the pre-eruption slow-rise phase can last several hours (Sterling *et al.* 2007), but it can be much shorter, ∼10 min for active-region eruptions (Schrijver *et al.* 2008). The slow-rise phase is followed by a rapid-acceleration phase ("fast-rise phase") during which velocities increase to a range of 100 to over 1000 km s^{-1}. The rapid-acceleration phase finally transitions into a phase with a nearly constant velocity or even a deceleration into the heliosphere.

However, previous studies are based on a single spacecraft which are influenced by projection effect. The launch of the twin *Solar Terrestrial Relations Observatory* (*STEREO*; Kaiser *et al.* 2008; Howard *et al.* 2008) spacecraft in October 2006 provided us an opportunity to view filament eruptions from two viewpoints giving new insights into their

three-dimensional (3D) geometry and true trajectory. Each spacecraft of the *STEREO* mission carries four remote sensing and in situ instrument suites. The Sun Earth Connection Coronal and Heliospheric Investigation (SECCHI; Howard *et al.* 2008) imaging package on each spacecraft consists of the following five telescopes: the EUVI imager, inner (COR1) and outer (COR2) coronagraphs, and inner (HI1) and outer (HI2) heliospheric imagers. EUVI images are taken at four wavelengths centered at 304 Å (6-8 × 10^4 K, primarily the He II line), 171 Å (10^6 K, primarily Fe IX/X), 195 Å (1.4 × 10^6 K, primarily Fe XII line) and 284 Å (2.2×10^6 K, Fe XV line). The standard SECCHI synoptic program provides simultaneous A-B image pairs at a ten min cadence for 304 Å and 195 Å and 2.5 min cadence for 171 Å. COR1 has a field of view (FOV) from 1.4 to 4 R_{sun} and COR2 from 2.5 to 15 R_{sun}.

In this paper, we mainly review the studies on filament reconstructions in the *STEREO* era. The reconstruction techniques are described in Section 2, the main results obtained from the analysis of *STEREO* EUVI data are described in Section 3 and the summary is presented in Section 4.

2. Reconstruction techniques

Since the launch of the *STEREO*, a few works have been published so far on the 3D reconstruction of filaments (Gissot *et al.* 2008; Liewer *et al.* 2009, 2013; Gosain *et al.* 2009; Li *et al.* 2010, 2011; Bemporad 2009, 2011). The main reconstruction techniques include the following three methods.

2.1. *Optical-flow algorithm*

The method of optical-flow algorithm was presented by Gissot *et al.* (2008) to reconstruct an erupting filament. This method is based on a novel algorithm which was developed to estimate displacement and brightness variation maps with *SOHO*/EIT data. Gissot *et al.* (2008) applied their algorithm to obtain the maps of the estimated apparent displacement of different parts of a filament due to different viewpoints in the *STEREO* A and B (304 Å) images. From the displacement maps, the radial distance from the solar center is derived pixel by pixel in EUVI images.

2.2. *Tie-pointing and triangulation*

The method of tie-pointing and triangulation is widely used by many authors to reconstruct erupting filaments (Liewer *et al.* 2009, 2013; Gosain *et al.* 2009; Li *et al.* 2010, 2011; Bemporad 2009, 2011; Joshi & Srivastava 2011). With this method, the same feature is identified in both images seen from different viewpoints, then the position of the feature in 3D coordinate system is determined by triangulation (Thompson 2006). This technique makes use of the epipolar geometry (Inhester 2006). The two observer positions and any object point to be reconstructed exactly define a plane, which is known as an epipolar plane. By definition, epipolar planes are projected on both observer's images as lines known as the epipolar lines. Once we identify a feature in one image, it is possible to determine the projection of the epipolar plane (i.e., epipolar line) passing the same feature in the second image, thus reducing the problem of placing the second tie-point from a 2D to 1D problem.

Many works mentioned above make use of the software tools for stereoscopy developed within the Solar Software library, in particular the scc_measure.pro routine (developed by W. Thompson). The routine uses triangulation to determine the 3D coordinate of the featured tie-pointed. It is a widget based application that allows the user to locate (and select with a cursor) the same feature in EUVI A and B images. Once the user selects a
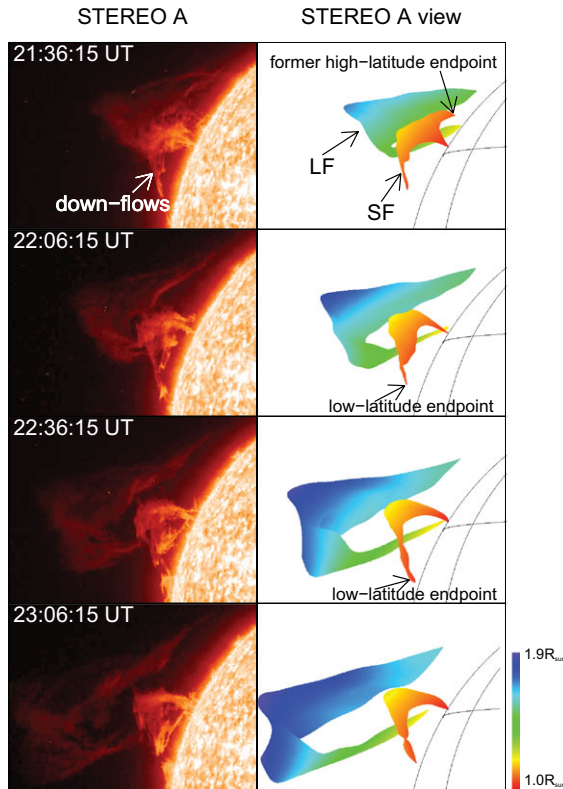
STEREO A   STEREO A view

Figure 1. Comparison of the observed filaments and reconstructed filaments seen from STEREO A view. Left: a series of STEREO A/EUVI 304 Å observed images showing the evolution of the filaments on 2009 Sep 26. Right: a series of reconstructed images seen from STEREO A showing the eruption process of the filaments. (Li *et al.* 2010)

feature in one image, immediately the epipolar line is displayed and the placement of the tiepoint in the second image is constrained to this line. After selecting the same feature in both images, the 3D coordinates of the feature are then determined as longitude, latitude, and radial distance from the center of the Sun.

2.3. *Tomographic method*

Gosain *et al.* (2012) recently developed a new tomographic method for the 3D reconstruction. The basic principle of this method is as follows. For the intensity image of the Sun such as in He II 304 Å, the same feature of a filament in *STEREO* A and B can be projected into heliographic coordinates. This projection is known as Marinus projection. If the heliographic projection is attempted (the Sun as a sphere with a larger radius than one solar radius) and a correct radius of the sphere is assumed, then the latitude and longitude of the common feature are the same. They generated the generalized Carrington maps for different assumed radius of the spherical grid, using a 5 Mm step from R = 700 Mm to R=1500 Mm, and compared the latitude-longitude positions of the same feature in three Carrington maps until they are the same. Then the 3D coordinate of the feature is obtained.

3. Results

From *STEREO* 3D reconstructions, the kinematic property and the twist or writhe of the filament could be obtained. Gosain *et al.* (2009) used mainly the tie-pointing technique and reconstructed the filament observed on 2008 May 22. They found that the filament sheet was not normal to the solar surface but highly inclined, with an inclination angle of about 47°. In Gosain & Schmieder (2010), they developed a new method for estimating the width and inclination of the filament by assuming that the filament is a rectangular sheet. They applied this method on the same filament analyzed by Gosain *et al.* (2009), and the inclination to the solar normal was estimated to be 54°, which is in good agreement with the results of their previous study by using the tie-pointing technique. Bemporad (2009) analyzed the 3D shape and orientation of the filament on 2007 May 9 and found that the filament can be approximated mainly as a 2D ribbon-like feature during the early expansion. In this work, the non-isotropic expansion was found because the expansion rate observed in the direction parallel to the filament plane was much larger than the expansion rate perpendicular to that plane.

The kinematical properties of filaments in 3D space could be obtained by reconstructing the featured points of the filaments. The height-time plot of the 3D trajectory of the filament material was initially presented by Liewer *et al.* (2009) which revealed evidence of a slow rise before the main eruption. The rapid rise from one to two solar radius immediately follows the flare peak.

A similar 3D height-time plot for the evolution of the filament was reported by Li *et al.* (2010). In this work, the velocities and accelerations in 3D space of different features along the filament axis were analyzed for the first time. It was found that the velocity and acceleration of features vary with the measured location. The highest points are not always the fastest as the points on the low-latitude leg later become the fastest. A new visualization method was applied after selecting a series of common features in EUVI A and B images by using the scc_measure.pro routine. This method is as follows. The top edge, the main-body line and the bottom edge are chosen as three baselines of the filaments. About 20 pairs of points are placed along each baseline. 500 points are interpolated by cubic spline along each baseline among the selected points to smooth the baseline. Then the enclosed region is simply filled in between any two baselines with 1000 triangular elements to produce the extended regions. Using this visualization method, the reconstructed filaments seen for any viewing angle can be displayed. The two reconstructed filaments seen from the *STEREO A* viewpoint on 2009 Sep 26 are shown in Figure 1. Colors denote different altitudes from the solar center. The two filaments almost simultaneously erupted and were thought to lie in the same filament channel. The latitudinal and longitudinal variations of the large filament are quite different, with the latitudinal motion faster than the longitudinal, which implies the non-isotropic eruption.

It is of great importance to apply different reconstruction techniques to the same event and compare the results. Gosain *et al.* (2012) recently applied their new tomographic method to the same filament as Li *et al.* (2010). The reconstruction from two independent methods agree quite well, considering the general scatter in the reconstructed coordinates. By fitting different functional forms to the true height-time profile of the filament apex during the rapid acceleration phase, they found that an exponential function fits the rise phase slightly better than parabolic or cubic functions.

With the increase of the separation angle between the two *STEREO* spacecraft, it is disadvantageous to reconstruct a 3D configuration of solar features by only using STEREO data. With the launch of the Solar Dynamics Observatory (SDO; Pesnell *et al.*

2012) in February 2010, 3D reconstruction would be improved by using observations of SDO and STEREO. Li *et al.* (2011) made use of observations from the three different viewpoints and reconstructed the 3D evolution process of a polar crown filament on 2010 August 01. It was found the filament moved towards the low-latitude region with a change in inclination by $\sim48°$ as the main body of the filament rose up. The filament expanded only in altitude and in the latitudinal direction, as also shown by Bemporad (2009). The feature at the highest location had the largest value of acceleration during this eruption process by investigating the true velocities and accelerations of different locations along the filament. Seen from the north pole, the velocity of the filament had a large Earth−directed component. This was consistent with the Earth−directed CME accompanying the eruptive filament.

The same event was also analyzed by Joshi & Srivastava (2011) and Chifu *et al.* (2012). In the work of Joshi & Srivastava (2011), they observed the variations in true longitude and latitude of the reconstructed features in the two legs of the filaments and attributed the variations to an interplay of two motions: the overall non-radial motion of the filament toward the equator and the helical twist in the filament spine. By studying the kinematics of the filament in the slow-rise and fast-eruptive phases, they found a constant acceleration for each reconstructed feature in each phase and the acceleration was found different for different features along the filaments. Chifu *et al.* (2012) found that the filament and CME core material did not evolve in a self-similar way.

Several authors analyzed the rotation motion of erupting filaments by reconstructing the 3D trajectory of the whole filament. Panasenco *et al.* (2010) analyzed three erupting filaments with sideways roll effect and found that all the erupting filaments and associated CMEs were non-radial and occurred near large coronal holes. The roll effect and non-radial motion were away from the closest coronal hole. Thompson (2011) derived the 3D structure of an erupting filament on 2007 June 5-6 and found that the filament underwent substantial rotation of at least $90°$ along the radial axis as it rose up. It was interpreted that the helical kink instability initiated the eruption and the counter-clockwise rotation of the filament.

Bemporad *et al.* (2011) investigated the filament on 2007 August 31 and showed evidence for a progressive clockwise rotation by about $90°$ during the filament eruption. Interestingly, the filament rotated by about $40°$ counter-clockwise in the week before the eruption and the overlying extrapolated potential field lines before the eruption rotated in the same direction as the rotation of the erupting filament. This suggested that the magnetic helicity storage occurred not only in the filament itself, but in the global magnetic field configuration of the surrounding corona. The same filament was also analyze by Liewer *et al.* (2013), who drew similar conclusions as Bemporad *et al.* (2011). They found that the filament rotation began in the slow rise phase and most of the rotation occurred in the fast rise phase, after the CME started to appear.

A larger rotation angle of the erupting filament was reported by Thompson *et al.* (2012), who revealed that the dextral filament rotated counter-clockwise by about $115°$ up to a height of 2.5 $R_\odot$ where the rotation leveled off. Zhu & Alexander (2013) reported the eruption of a bifurcated filament and found that the upper branch of the filament rotated approximately $120°$ in a counter-clockwise direction. Bi *et al.* (2013) analyzed the simultaneous non-radial and rotation motion of the filament axis by reconstructing the 3D geometry of the filament and suggested that the non-radial motion was influenced by the overlying pseudostreamer and the rotation motion was a representation of the asymmetric deflection between the eastern and western segments of the filament.

4. Summary

By reconstructing the 3D eruption process of filaments with *STEREO* data, the kinematical parameters (velocity and acceleration vectors), rotation motion, non-radial motion and helical twist around the filament axis have been studied in the past several years. However, the full potential of *STEREO* data in addressing many open questions, such as the eruption mechanism of filaments and CMEs, has not been utilized so far. It is therefore necessary to combine *STEREO* observations with data from other ground-based and space-based solar observatories for exploring the physical nature of filament eruptions.

References

Antiochos, S. K., DeVore, C. R., & Klimchuk, J. A. 1999, *ApJ*, 510, 485
Bemporad, A. 2009, *ApJ*, 701, 298
Bemporad, A. 2011, *Journal of Atmospheric and Solar-Terrestrial Physics*, 73, 1117
Bemporad, A., Mierla, M., & Tripathi, D. 2011, *A&A*, 531, A147
Bi, Y., Jiang, Y., Yang, J., *et al.* 2013, *ApJ*, 773, 162
Chifu, I., Inhester, B., Mierla, M., Chifu, V., & Wiegelmann, T. 2012, *Sol. Phys.*, 281, 121
Fan, Y. 2005, *ApJ*, 630, 543
Filippov, B. 2013, *ApJ*, 773, 10
Gilbert, H. R., Alexander, D., & Liu, R. 2007, *Sol. Phys.*, 245, 287
Gissot, S. F., Hochedez, J.-F., Chainais, P., & Antoine, J.-P. 2008, *Sol. Phys.*, 252, 397
Gosain, S. & Schmieder, B. 2010, *Annales Geophysicae*, 28, 149
Gosain, S., Schmieder, B., Artzner, G., Bogachev, S., & Török, T. 2012, *ApJ*, 761, 25
Gosain, S., Schmieder, B., Venkatakrishnan, P., Chandra, R., & Artzner, G. 2009, *Sol. Phys.*, 259, 13
Howard, R. A., Moses, J. D., Vourlidas, A., *et al.* 2008, *Space Sci. Riv.*, 136, 67
Illing, R. M. E. & Hundhausen, A. J. 1986, *JGR*, 91, 1095
Inhester, B. 2006, arXiv:astro-ph/0612649
Jiang, Y., Yang, J., Hong, J., Bi, Y., & Zheng, R. 2011, *ApJ*, 738, 179
Joshi, A. D. & Srivastava, N. 2011, *ApJ*, 730, 104
Kahler, S. W., Moore, R. L., Kane, S. R., & Zirin, H. 1988, *ApJ*, 328, 824
Kaiser, M. L., Kucera, T. A., Davila, J. M., *et al.* 2008, *Space Sci. Riv.*, 136, 5
Kliem, B. & Török, T. 2006, *Physical Review Letters*, 96, 255002
Li, T. & Zhang, J. 2013, *ApJL*, 770, L25
Li, T., Zhang, J., Zhang, Y., & Yang, S. 2011, *ApJ*, 739, 43
Li, T., Zhang, J., Zhao, H., & Yang, S. 2010, *ApJ*, 720, 144
Liewer, P. C., de Jong, E. M., Hall, J. R., Howard, R. A., Thompson, W. T., Culhane, J. L., Bone, L., & van Driel-Gesztelyi, L. 2009, *Sol. Phys.*, 256, 57
Liewer, P. C., Panasenco, O., & Hall, J. R. 2013, *Sol. Phys.*, 282, 201
Liu, R., Kliem, B., Török, T., *et al.* 2012, *ApJ*, 756, 59
Moore, R. L., Sterling, A. C., Hudson, H. S., & Lemen, J. R. 2001, *ApJ*, 552, 833
Panasenco, O., Martin, S., Joshi, A. D., & Srivastava, N. 2011, *Journal of Atmospheric and Solar-Terrestrial Physics*, 73, 1129
Pesnell, W. D., Thompson, B. J., & Chamberlin, P. C. 2012, *Sol. Phys.*, 275, 3
Schrijver, C. J., Elmore, C., Kliem, B., *et al.* 2008, *ApJ*, 674, 586
Shen, Y., Liu, Y., & Su, J. 2012, *ApJ*, 750, 12
Sterling, A. C., Harra, L. K., & Moore, R. L. 2007, *ApJ*, 669, 1359

Sturrock, P. A. 1989, *Sol. Phys.*, 121, 387

Tandberg-Hanssen, E., Martin, S. F., & Hansen, R. T. 1980, *Sol. Phys.*, 65, 357

Thompson, W. T. 2006, *A&A*, 449, 791

Thompson, W. T. 2011, *Journal of Atmospheric and Solar-Terrestrial Physics*, 73, 1138

Thompson, W. T., Kliem, B., & Török, T. 2012, *Sol. Phys.*, 276, 241

Török, T. & Kliem, B. 2005, *ApJL*, 630, L97

Zhu, C. & Alexander, D. 2013, *Sol. Phys.*, 200